Industrial Chemistry & Materials

ROYAL SOCIETY OF CHEMISTRY

PAPER

View Article Online
View Journal | View Issue

Cite this: *Ind. Chem. Mater.*, 2023, **1**, 140

Supercritical CO_2-induced room-temperature ferromagnetism in two-dimensional MoO_{3-x}†

Wei Liu [a] and Qun Xu *[ab]

Two-dimensional (2D) magnetic semiconductors are crucial in spin-based information-processing technologies due to the combination of the strong 2D quantum effects, surface effects and the control of spin states. However, most experimental approaches for tuning 2D magnets achieve pure ferromagnetism at low temperature. Herein, a defect engineering strategy using supercritical CO_2 is introduced to achieve nanostructure with abundant defects for 2D MoO_{3-x}, and room-temperature ferromagnetism can be obtained and tuned by introduction of the Mo^{5+} ion depending on the change of supercritical pressure. In defective regions, the presence of the pentacoordinated [$Mo^{5+}O_5$] centers can achieve ferromagnetic ordering resulting in room-temperature ferromagnetism. With increasing supercritical pressure, it is easier for the supercritical CO_2 to break the Mo–O bonds, achieving enhancement of the ferromagnetic performance with desired Curie temperature (>380 K). The magnetic responses in the MoO_{3-x} system provide a step closer to the expansion of spin electronics.

Received 21st September 2022,
Accepted 25th November 2022

DOI: 10.1039/d2im00028h

rsc.li/icm

Keywords: Supercritical CO_2; Room-temperature ferromagnetism; Two-dimensional; MoO_{3-x}.

1 Introduction

Room-temperature two-dimensional ferromagnets are at the forefront of research owing to the unusual physical and chemical properties that are useful for various applications, especially spintronics.[1–3] In recent years, vigorous scientific inquiry has been undertaken on magnetic semiconductors, which possess both semiconductor and magnetic properties.[4–7] 2D transition-metal dichalcogenides (TMDs) and oxides (TMOs) with strong spin–orbit coupling are foreseen as promising candidates, such as MoS_2, WS_2, VSe_2, VS_2, ZnO and Ti_2O_3.[8–13] However, because of the weak magnetic coupling or a lack of unpaired electrons, most of the pristine TMDs and TMOs are intrinsically nonmagnetic. Hence, exploring experimental approaches to modulate the magnetism are being pursued.

To date, systematic structural modulation methods to induce the signature of magnetic ordering are mainly classified as substitutional doping, phase transition, formation of surface dangling bonds, strain engineering and introduction of vacancies or defects.[14–16] Among various 2D TMOs, because of tunable electrical properties, MoO_3 has become attractive for achieving modulation of magnetic behavior. For example, room-temperature ferromagnetism of MoO_3 was achieved by manipulating nanostructures such as nanofibers and hierarchical branches.[17,18] And transition metal elements and non-metal elements doping can help the fabrication of ferromagnetism in Co-doped MoO_3 films, and Ni- and Ni–Co doped MoO_3 films, Te-doped MoO_3 nanoflakes and hydrogen-doped MoO_3 nanosheets.[19–22] Due to the absence of unpaired electron spins, stoichiometric MoO_3 and MoO_2 are reported to be paramagnetic semiconductors.[23] To expand the multifunctionality of spintronics devices where charge and spin manipulation could be combined, such as the novel magnetic tunnel junction, semiconductors with desirable magnetic nature have become more important; desirable properties include high saturation magnetization (M_s) under lower magnetic field, low coercivity field (H_c) and high Curie temperature (T_c).[24] In fact, ferromagnetism can be manipulated by controlling the defects in 2D nanostructure, such as different magnetic properties depending on various defects in graphitic carbon.[25–27]

In supercritical fluid technology, as a green industrial solvent system, supercritical CO_2 (SC CO_2) can exfoliate various 2D layered materials, and in the interlayer confined space, CO_2 can prompt diffusive atomic disordering to control the formation of defects because the generated local stress acts on the 2D surface.[28,29] Defects strategy is beneficial for the introduction of unpaired electrons into the system, which is expected as an effective technical means to obtain 2D materials with ferromagnetic properties. Recently,

[a] *Henan Institute of Advanced Technology, Zhengzhou University, Zhengzhou 450001, P.R. China. E-mail: qunxu@zzu.edu.cn*
[b] *Department of Materials Science and Engineering, Zhengzhou University, Zhengzhou 450001, P.R. China*

† Electronic supplementary information (ESI) available. See DOI: https://doi.org/10.1039/d2im00028h

non-van der Waals-like layered VO_2 and $BaTiO_3$ materials have exhibited superior ferromagnetism because of the induced symmetry breaking after high pressure treatment with SC CO_2.[30,31] Herein, for the first time, we report the successful fabrication of ferromagnetic 2D MoO_{3-x} nanosheets with the assistance of SC CO_2. And the magnetic moments in the defect regions result in ferromagnetic responses and the saturation magnetization reaches 0.01 emu g^{-1} under ~2000 Oe magnetic field at room temperature, and the Curie temperature can reach to over 380 K.

2 Results and discussion

To verify the atomic arrangement of MoO_{3-x}, transmission electron microscopy (TEM) is applied to observe the surface morphology. From the TEM image in Fig. 1a, the 2D sheet-like structure with irregular contour can be clearly visualized. The high resolution transmission electron microscopy (HRTEM) image (Fig. 1b) taken of the MoO_{3-x} nanosheet shows an imperfect atomic arrangement with a (110) lattice distance of 0.38 nm. The ordered crystal lattices are separated by disordered regions. The fast Fourier transform (FFT) pattern also exhibits well-defined orthorhombic rings spots, which is consistent with layered α-MoO_{3-x}. Moreover, according to the atomic force microscopy (AFM) analysis in Fig. 1c, the exfoliated MoO_{3-x} nanosheets have a thickness of ~4.5 nm (5–6 layers).[32,33] The corresponding energy dispersive X-ray (EDX) elemental mapping images (Fig. 1d and e) further suggest the uniform distribution of Mo and O elements on the sheets. Thus, SC CO_2 can destroy the Mo–O bonds on the surface, forming large amounts of defects and vacancies (Fig. 1f).

The MoO_{3-x} shows abundant defects, which can be proven by the X-ray diffraction (XRD) patterns (Fig. 2a). Its X-ray powder diffraction pattern has a broad peak curve in the range of 20 to 30°, suggesting the existence of a disordered structure. Raman measurements at a low laser power were carried out (excitation wavelength: 532 nm). As can be seen in Fig. 2b, strong peaks occur at 818 and 991 cm^{-1} for the sample. The 818 cm^{-1} peak is assigned to the doubly coordinated oxygen (Mo_2–O) stretching mode, and the peak at 991 cm^{-1} is attributable to the terminal oxygen (Mo═O) stretching mode. Other peaks at 334 and 374 cm^{-1} can be assigned to Mo_3–O and Mo═O bending modes. And the broad trends of these peaks show the existence of lattice defects or the local disorder in MoO_{3-x}.[34,35] To elucidate the elemental composition and oxidation state of the MoO_{3-x}, X-ray photoelectron spectroscopy (XPS) measurements were performed. For the XPS spectrum of Mo 3d, peaks correspond to Mo^{6+} (236.0 and 232.8 eV) and Mo^{5+} (234.8 and 231.6 eV), respectively (Fig. 2c).[36,37] The proportion of Mo^{5+} can reach as high as 14.9%. The coexistence of Mo^{6+} and Mo^{5+} verifies the existence of oxygen vacancies. Fig. 2d shows the O 1s spectrum, the peaks at 530.5 eV and 532.4 eV correspond to

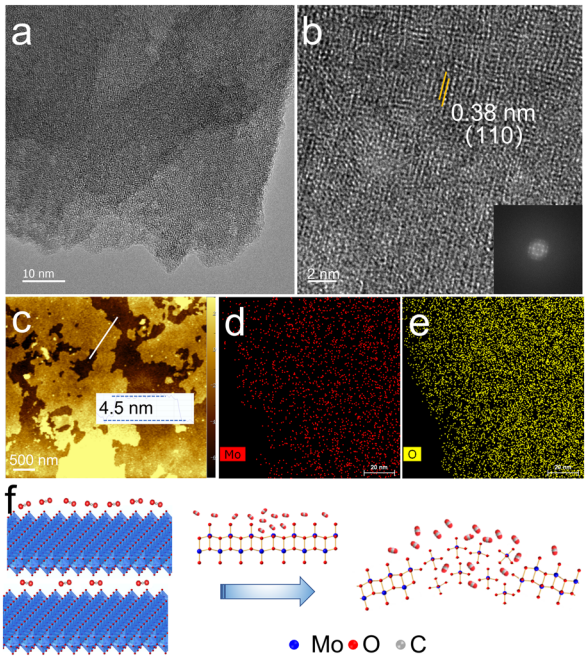

Fig. 1 (a) TEM image of the MoO_{3-x} nanosheets; (b) HRTEM image of the MoO_{3-x} nanosheets, inset: the corresponding fast Fourier transform (FFT) pattern; (c) AFM image of the MoO_{3-x} nanosheets; (d and e) elemental mapping of the MoO_{3-x} nanosheets for Mo and O; (f) schematic side views showing the formation of MoO_{3-x} using SC CO_2. Mo, O, and C atoms are represented by balls in blue, red, and grey, respectively.

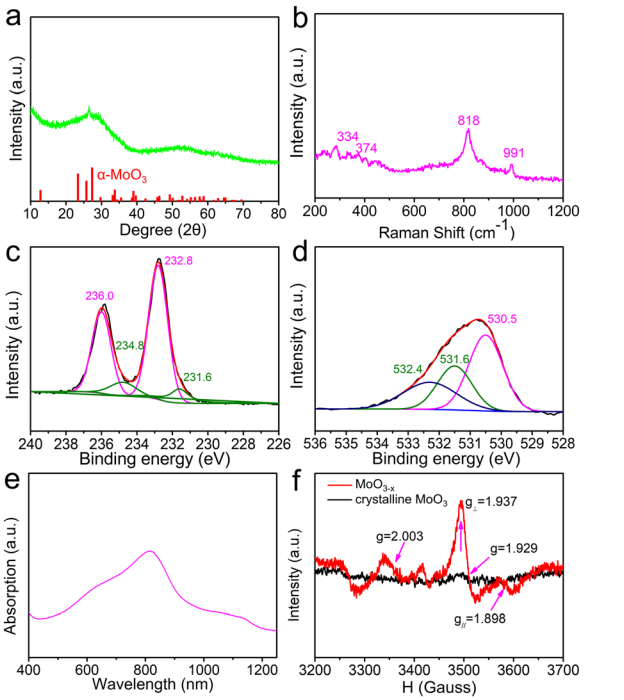

Fig. 2 (a) XRD patterns of the MoO_{3-x} nanosheets; (b) Raman scattering characteristics of the MoO_{3-x} nanosheets; (c and d) XPS spectrum details of MoO_{3-x} for Mo 3d and O 1s binding energy regions; (e) absorption spectrum of MoO_{3-x} (concentration: 1 mg mL^{-1}); (f) EPR spectrum of the MoO_{3-x} nanosheets.

oxygen in MoO_6 and surface adsorbed species, respectively.[38,39] And the energy level (531.6 eV) also suggests the existence of neighbouring oxygen vacancies.[40] From the absorption spectrum of MoO_{3-x}, the absorption in the visible–near infrared regions consists of three peaks at 685, 815 and 1050 nm, corresponding to 1.8, 1.5 and 1.2 eV, respectively. The three peaks originate from the intervalence charge transfer, the d–d transitions of Mo^{5+} and the surface plasmon resonance (SPR) of the MoO_{3-x} nanosheets (Fig. 2e).[41] It is concluded that the surface of MoO_{3-x} possesses enough unsaturated atoms, resulting from oxygen vacancies.[42,43] In order to investigate the oxygen vacancies and coordinately unsaturated Mo^{5+} atoms in Mo–O tetragonal pyramids of the MoO_{3-x} nanosheets, electron paramagnetic resonance (EPR) spectrum measurements were carried out. Fig. 2f shows the hyperfine structure of Mo^{5+} with sharp peaks of parallel ($g_{\parallel}$ = 1.898) and perpendicular ($g_{\perp}$ = 1.937) bands and oxygen vacancies (g = 2.003), while these weakened peaks in crystalline MoO_3 account for few unsaturated atoms.[33]

The photoluminescence (PL) spectrum at 300 K of the MoO_{3-x} nanosheets is shown in Fig. 3a. Compared with crystalline MoO_3, the PL spectrum of MoO_{3-x} exhibits obvious emission and a blue-green emission peak centred at about 510 nm, which originates from the presence of the singly charged oxygen vacancy (V_o^+).[17] V_o^+ defects with unpaired electrons can be the source of ferromagnetism, because they limit delocalization of unpaired electrons potentially giving rise to ferromagnetic double exchange. Owing to the inherent properties of layered MoO_{3-x}, the net magnetic moment can be localized on the d orbital of the Mo atom.[17] Moreover, the asymmetric nature of the photoluminescence spectrum at higher wavelengths can be ascribed to the intraband transitions occurring at the pentacoordinated [$Mo^{5+}O_5$] centers.[19]

The magnetic properties of the MoO_{3-x} nanosheets were studied by measuring the magnetization as a function of applied magnetic field (M–H) at 300 K. From Fig. 3b and c, the magnetic response of the sample with S-shaped and linear forms of the hysteresis loop shows ferromagnetic responses. Particularly, the ferromagnetic behavior is observed for low values of the magnetic excitation up to ~2000 Oe. And the M_s is about 0.01 emu g^{-1}. The magnified curves near H = 0 show that H_c and the remnant magnetization (M_r) are about 52 Oe and 0.001 emu g^{-1}. As can be confirmed from Fig. 3d, the magnetization *vs.* temperature (M–T) curves further substantiate room-temperature ferromagnetism in MoO_{3-x} nanosheets, and the zero-field-cooled (ZFC) and field-cooled (FC) curves show obvious splitting over the whole measurement temperature range, indicating the Curie temperature (T_C) is >380 K.[19] To compare with the reported oxide series (MoO_3–MoO_{3-x}–MoO_2) and their doped compounds, the experimental magnetic parameters at room temperature are given in Table S1 (see ESI†). The M_s, M_r and T_c of the as-prepared MoO_{3-x} are outstanding, meanwhile, H_c can maintain a low value. Importantly, the yield is around 10%, and the preparation process is expected to recycle CO_2 for the large-scale production of ferromagnetic MoO_{3-x}, which has potential for practical applications.

To further identify the magnetic source, it is necessary to study the magnetic properties of SC CO_2-treated samples at different pressures. The XRD patterns (Fig. 4a) show that the crystal structure of the nanosheets is more disordered with an increase in SC CO_2 pressure except for that of 16 MPa, owing to a phase transition into the hexagonal phase for MoO_{3-x} (h-MoO_{3-x}).[44] Moreover, from their corresponding HRTEM images (Fig. 4b–d), it can be found that the atomic arrangements are all more perfect than that of the MoO_{3-x}

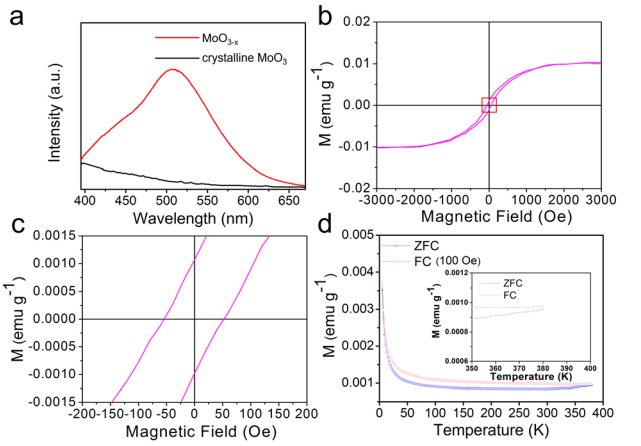

Fig. 3 (a) PL emission spectra at 300 K of the MoO_{3-x} nanosheets and crystalline MoO_3 excited at 365 nm; (b) magnetization hysteresis loop of the MoO_{3-x} nanosheets at 300 K; (c) the magnified curves near H = 0; (d) M–T curves of the MoO_{3-x} nanosheets measured under ZFC and FC (H = 100 Oe) modes.

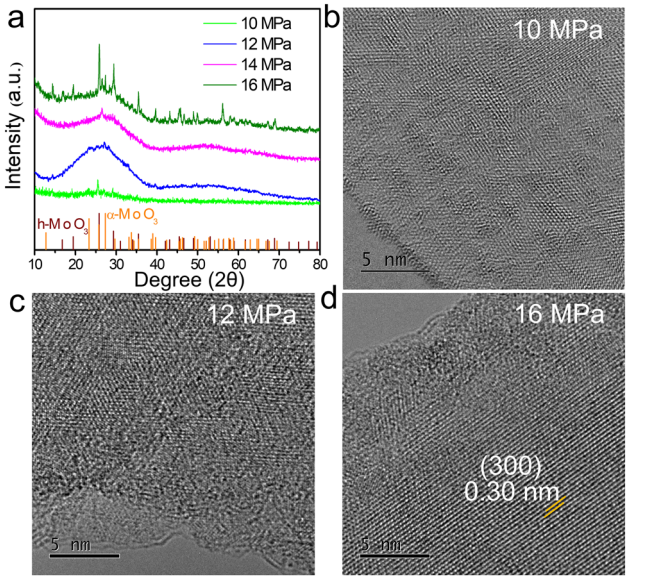

Fig. 4 (a) XRD patterns comparison of the MoO_{3-x} obtained at different pressures, and XRD patterns at the bottom show α-MoO_3 (JCPDS No. 05-0508) and h-MoO_3 (JCPDS No. 21-0569); (b–d) HRTEM images of the MoO_{3-x} sample obtained at 10 MPa, 12 MPa, 16 MPa.

obtained at 14 MPa. Among them, the lowest degree of defects can be found for MoO_{3-x} obtained at 10 MPa, which indicates the SC CO_2 destroys the atomic arrangement under high enough pressure conditions. Additionally, h-MoO_{3-x} with a (300) lattice distance of 0.30 nm for the 16 MPa sample is observed clearly, which is agreeing with the XRD results. In addition, the variation of atomic structures is also analyzed by XPS. From the XPS spectrum analysis (Fig. 5), compared to that of samples obtained at 14 MPa (14.9%), the proportions of Mo^{5+} for MoO_{3-x} obtained at 10, 12 and 16 MPa are 5.2%, 9.2% and 14.6% respectively, which demonstrates the introduction of more Mo^{5+} with increase in SC CO_2 pressure. It is known that the Mo^{5+} ion has an unpaired electron spin (*i.e.*, Mo^{5+}: [Kr]$4d^1$), so the presence of the pentacoordinated [$Mo^{5+}O_5$] centers can also provide net magnetic moments in addition to the introduction of the oxygen vacancies in MoO_3.[19]

In addition, the variation trend of the Mo^{5+} component is also partly reflected in their EPR spectra (Fig. 6a). It can be observed that the unpaired electron spin signal strength of Mo^{5+} in the samples becomes strong with the increase in pressure, and 14 MPa is the strongest when compared. And there are no obvious signal responses of oxygen vacancies for these samples obtained at 10, 12 and 16 MPa, which could be disadvantageous to ferromagnetic performance. Further, their magnetic behaviors are also confirmed by *M–H* loop measurements (Fig. 6b), and it shows a paramagnetic response for crystalline MoO_3, differing from the ferromagnetism of the MoO_{3-x} obtained at 12, 14 and 16 MPa.

It is concluded that both Mo^{5+} and oxygen vacancies contribute to the achievement of ferromagnetism, which can be tuned by SC CO_2 pressure, because the bound magnetic polarons could be formed *via* Mo^{5+} coupling with the charged oxygen vacancies.[18] Meanwhile, the M_s and M_r reduce remarkably for the sample at 16 MPa (Fig. S1†), which shows the necessity of 2D structure. Moreover, there is less Mo^{5+} and a weak ferromagnetic response for the MoO_{3-x} nanosheets obtained by sonication treatment without SC CO_2 (Fig. S2†). Therefore, through defect engineering by SC CO_2, the Mo^{5+} can induce polarized spins, which is critical to the magnetic properties for 2D molybdenum oxide materials.

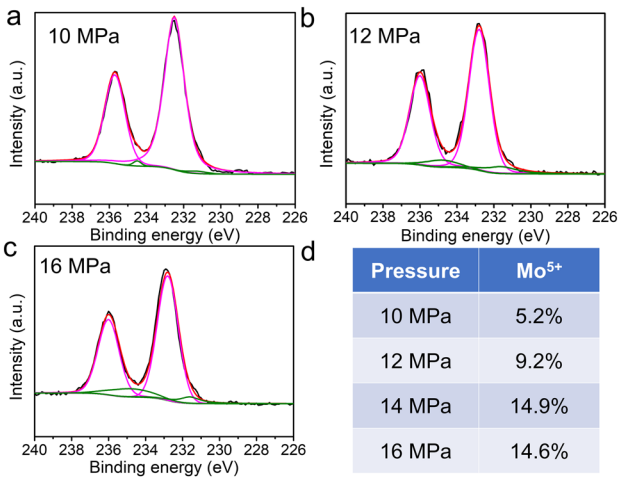

d

Pressure	Mo^{5+}
10 MPa	5.2%
12 MPa	9.2%
14 MPa	14.9%
16 MPa	14.6%

Fig. 5 (a–c) XPS spectrum details of the Mo 3d binding energy regions and (d) the varied percent of Mo^{5+} for the MoO_{3-x} sample obtained at 10 MPa, 12 MPa, 16 MPa.

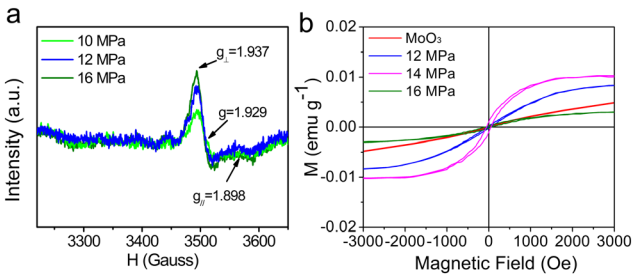

Fig. 6 (a) EPR spectra comparison of MoO_{3-x} obtained at different pressures; (b) magnetization hysteresis loop comparison of the MoO_{3-x} sample obtained at 12 MPa, 14 MPa, 16 MPa and crystalline MoO_3 at 300 K.

3 Conclusions

In summary, a defect engineering strategy using SC CO_2 is presented to endow nonmagnetic 2D materials with ferromagnetic properties. The 2D MoO_{3-x} nanosheets are selected as a model, in which the introduction of moderate Mo^{5+} provides the MoO_{3-x} nanosheets with ferromagnetic behavior at room temperature, resulting from magnetic polarons in defective regions. And the MoO_{3-x} nanosheets exhibit a large saturation magnetization (0.01 emu g^{-1}) and T_C (>380 K). Moreover, SC CO_2 can tune the magnetic properties achieving continuous enhancement of ferromagnetic performance with increasing supercritical CO_2 pressure below the phase transformation pressure, and 14 MPa is the optimum pressure. Undoubtedly, the strategy is feasible to stimulate the ferromagnetic characteristics of other kinds of 2D materials for more capabilities and higher performances of spintronics devices in complex magnetic environments.

4 Experimental section

4.1 Materials and methods

4.1.1 Materials. MoS_2 powder was purchased from Sigma-Aldrich (Fluka, product number 69860). Analytical grade ethanol was provided by Sinopharm Chemical Reagent Co., Ltd. All were directly used owing to their analytical grade. CO_2 with a purity of 99.99% was purchased from the Zhengzhou Shuangyang Gas Co. Deionized water was prepared with double-distilled water.

4.1.2 Preparation of MoO_{3-x} nanosheets. MoS_2 powder (100 mg) was first annealed at 623 K for 90 min in the air. The obtained MoO_3 was dispersed in a 45% ethanol/water mixture (10 mL) and subsequently was sonicated for 1 h in a water bath (equipment power: 200 W), forming a uniform black dispersion. Then the dispersion was quickly transferred into the supercritical CO_2 apparatus composed

mainly of a stainless-steel autoclave with a heating jacket and a temperature controller. The autoclave was heated to 353 K, and then CO_2 was charged into reactor to the set pressure (*e.g.* 10, 12, 14 and 16 MPa). The autoclave was maintained at 353 K for 3 h and then cooled to room temperature. The dispersion was centrifuged at 6000 rpm for 15 min to remove aggregates, and the supernatant was collected. Then the solution was dried in an oven at a constant temperature of 333 K.

4.1.3 Characterization. TEM images were obtained on a JEOL JEM 2100F transmission electron microscope at an acceleration voltage of 200 kV. The XRD patterns were examined using a Bruker D8 Advance diffractometer using germanium monochromatic CuKα radiation (40 kV and 40 mA). The thickness of the nanosheets was measured using AFM (NanoManVS). Raman spectra of the samples were measured using a LabRAM HR Evolution with 532 nm laser excitation. XPS measurements were performed on a Thermo ESCALAB 250XI platform. Magnetic properties were characterized using a superconducting quantum interference device (SQUID)-magnetic property measurement system (MPMS)-3. UV–vis–NIR spectroscopy was carried out with a Shimadzu UV-240/PC. The PL spectra were recorded at room temperature on a Hitachi F-4500 spectrophotometer.

Conflicts of interest

There are no conflicts to declare.

Acknowledgements

We are grateful to the National Natural Science Foundation of China (No. 21773216, 51173170), the Henan-Provincial and the China-National Natural Science United Foundation (Project No. U2004208).

References

1 K. S. Burch, D. Mandrus and J. G. Park, Magnetism in two-dimensional van der Waals materials, *Nature*, 2018, **563**, 47–52.
2 Y. Liu, J. Guo, A. Yu, Y. Zhang, J. Kou, K. Zhang, R. Wen, Y. Zhang, J. Zhai and Z. L. Wang, Magnetic-induced-piezopotential gated MoS_2 field-effect transistor at room temperature, *Adv. Mater.*, 2018, **30**, 1704524.
3 W. Wang, M. W. Daniels, Z. Liao, Y. Zhao, J. Wang, G. Koster, G. Rijnders, C.-Z. Chang, D. Xiao and W. Wu, Spin chirality fluctuation in two-dimensional ferromagnets with perpendicular magnetic anisotropy, *Nat. Mater.*, 2019, **18**, 1054–1059.
4 M. Gibertini, M. Koperski, A. F. Morpurgo and K. S. Novoselov, Magnetic 2D materials and heterostructures, *Nat. Nanotechnol.*, 2019, **14**, 408–419.
5 T. Song, Z. Fei, M. Yankowitz, Z. Lin, Q. Jiang, K. Hwangbo, Q. Zhang, B. Sun, T. Taniguchi, K. Watanabe, M. A. McGuire, D. Graf, T. Cao, J.-H. Chu, D. H. Cobden, C. R. Dean, D. Xiao and X. Xu, Switching 2D magnetic states via pressure tuning of layer stacking, *Nat. Mater.*, 2019, **18**, 1298–1302.
6 N. Sivadas, S. Okamoto, X. Xu, C. J. Fennie and D. Xiao, Stacking-dependent magnetism in bilayer CrI_3, *Nano Lett.*, 2018, **18**, 7658–7664.
7 M. Bonilla, S. Kolekar, Y. Ma, H. C. Diaz, V. Kalappattil, R. Das, T. Eggers, H. R. Gutierrez, M.-H. Phan and M. Batzill, Strong room-temperature ferromagnetism in VSe_2 monolayers on van der Waals substrates, *Nat. Nanotechnol.*, 2018, **13**, 289–293.
8 W. Yu, J. Li, T. S. Herng, Z. Wang, X. Zhao, X. Chi, W. Fu, I. Abdelwahab, J. Zhou, J. Dan, Z. Chen, Z. Chen, Z. Li, J. Lu, S. J. Pennycook, Y. P. Feng, J. Ding and K. P. Loh, Chemically exfoliated VSe_2 monolayers with room-temperature ferromagnetism, *Adv. Mater.*, 2019, **31**, 1903779.
9 Y. Li, Y. Weng, X. Yin, X. Yu, S. R. S. Kumar, N. Wehbe, H. Wu, H. N. Alshareef, S. J. Pennycook, M. B. H. Breese, J. Chen, S. Dong and T. Wu, Orthorhombic Ti_2O_3: a polymorph-dependent narrow-bandgap ferromagnetic oxide, *Adv. Funct. Mater.*, 2018, **28**, 1705657.
10 H. Tan, C. Wang, W. Hu, H. Duan, P. Guo, N. Li, G. Li, L. Cai, Z. Sun, F. Hu and W. Yan, Reversible tuning of the ferromagnetic behavior in Mn-doped MoS_2 nanosheets via interface charge transfer, *ACS Appl. Mater. Interfaces*, 2018, **10**, 31648–31654.
11 Y. Guo, H. Deng, X. Sun, X. Li, J. Zhao, J. Wu, W. Chu, S. Zhang, H. Pan, X. Zheng, X. Wu, C. Jin, C. Wu and Y. Xie, Modulation of metal and insulator states in 2D ferromagnetic VS_2 by van der Waals interaction engineering, *Adv. Mater.*, 2017, **29**, 1700715.
12 T. Taniguchi, K. Yamaguchi, A. Shigeta, Y. Matsuda, S. Hayami, T. Shimizu, T. Matsui, T. Yamazaki, A. Funatstu, Y. Makinose, N. Matsushita, M. Koinuma and Y. Matsumoto, Enhanced and engineered d^0 ferromagnetism in molecularly-thin zinc oxide nanosheets, *Adv. Funct. Mater.*, 2013, **23**, 3140–3145.
13 J. Luxa, O. Jankovsky, D. Sedmidubsky, R. Medlin, M. Marysko, M. Pumera and Z. Sofer, Origin of exotic ferromagnetic behavior in exfoliated layered transition metal dichalcogenides MoS_2 and WS_2, *Nanoscale*, 2016, **8**, 1960–1967.
14 R. Sanikop and C. Sudakar, Tailoring magnetically active defect sites in MoS_2 nanosheets for spintronics applications, *ACS Appl. Nano Mater.*, 2020, **3**, 576–587.
15 S. Yan, W. Qiao, X. He, X. Guo, L. Xi, W. Zhong and Y. Du, Enhancement of magnetism by structural phase transition in MoS_2, *Appl. Phys. Lett.*, 2015, **106**, 012408.
16 Z. Zhang, X. Zou, V. H. Crespi and B. I. Yakobson, Intrinsic magnetism of grain boundaries in two-dimensional metal dichalcogenides, *ACS Nano*, 2013, **7**, 10475–10481.
17 S. K. S. Patel, K. Dewangan and N. S. Gajbhiye, Synthesis and room temperature d^0 ferromagnetic properties of α-MoO_3 nanofibers, *J. Mater. Sci. Technol.*, 2015, **31**, 453–457.
18 Y. Mao, W. Li, X. Sun, Y. Ma, J. Xia, Y. Zhao, X. Lu, J. Gan, Z. Liu, J. Chen, P. Liu and Y. Tong, Room-temperature ferromagnetism in hierarchically branched MoO_3 nanostructures, *CrystEngComm*, 2012, **14**, 1419–1424.

19 D. J. Lee, Y. Lee, Y. H. Kwon, S. H. Choi, W. Yang, D. Y. Kim and S. Lee, Room-temperature ferromagnetic ultrathin α-MoO_3:Te nanoflakes, *ACS Nano*, 2019, **13**, 8717–8724.

20 O. Kamoun, A. Boukhachem, S. Alleg, B. Jeyadevan and M. Amlouk, Physical study of nano-structured MoO_3 films codoped with cobalt and nickel in which there is a ferro-diamagnetic transition, *J. Alloys Compd.*, 2018, **741**, 847–854.

21 J. Zhang, J. Fu, F. Shi, Y. Peng, M. Si, L. Cavallo and Z. Cao, Hydrogen atom induced magnetic behaviors in two-dimensional materials: insight on origination in the model of α-MoO_3, *Nanoscale*, 2018, **10**, 14100–14106.

22 A. Boukhachem, M. Mokhtari, N. Benameur, A. Ziouche, M. Martínez, P. Petkova, M. Ghamnia, A. Cobo, M. Zergoug and M. Amlouk, Structural optical magnetic properties of Co doped α-MoO_3 sprayed thin films, *Sens. Actuators, A*, 2017, **253**, 198–209.

23 M. A. Khilla, H. Mikhail, A. A.-E. Soud and Z. M. Hanafi, Magnetic susceptibility of molybdenum trioxide, dioxide and some suboxides, *Czech. J. Phys. B*, 1980, **30**, 1039–1045.

24 C. Gong and X. Zhang, Two-dimensional magnetic crystals and emergent heterostructure devices, *Science*, 2019, **363**, eaav4450.

25 S.-M. Jung, J. Park, D. Shin, H. Y. Jeong, D. Lee, I.-Y. Jeon, H. Cho, N. Park, J.-W. Yoo and J.-B. Baek, Paramagnetic carbon nanosheets with random hole defects and oxygenated functional groups, *Angew. Chem., Int. Ed.*, 2019, **58**, 11670–11675.

26 R. R. Nair, M. Sepioni, I. L. Tsai, O. Lehtinen, J. Keinonen, A. V. Krasheninnikov, T. Thomson, A. K. Geim and I. V. Grigorieva, Spin-half paramagnetism in graphene induced by point defects, *Nat. Phys.*, 2012, **8**, 199–202.

27 J. Červenka, M. I. Katsnelson and C. F. J. Flipse, Room-temperature ferromagnetism in graphite driven by two-dimensional networks of point defects, *Nat. Phys.*, 2009, **5**, 840–844.

28 W. Liu, Q. Xu, W. Cui, C. Zhu and Y. Qi, CO_2-assisted fabrication of two-dimensional amorphous molybdenum oxide nanosheets for enhanced plasmon resonances, *Angew. Chem., Int. Ed.*, 2017, **56**, 1600–1604.

29 Y. Ren, C. Li, Q. Xu, J. Yan, Y. Li, P. Yuan, H. Xia, C. Niu, X. Yang and Y. Jia, Two-dimensional amorphous heterostructures of Ag/a-WO_{3-x} for high-efficiency photocatalytic performance, *Appl. Catal., B*, 2019, **245**, 648–655.

30 Y. Zhou, P. Yan, S. Zhang, C. Ma, T. Ge, X. Zheng, L. Zhang, J. Jiang, Y. Shen, J. Chen and Q. Xu, Conversion of non-van der Waals VO_2 solid to 2D ferromagnet by CO_2-induced phase engineering, *Nano Today*, 2021, **40**, 101272.

31 B. Gao, S. Xu and Q. Xu, CO_2-induced exposure of the intrinsic magnetic surface of $BaTiO_3$ to give room-temperature ferromagnetism, *Angew. Chem.*, 2022, **61**, e202117084.

32 I. A. de Castro, R. S. Datta, J. Z. Ou, A. Castellanos-Gomez, S. Sriram, T. Daeneke and K. Kalantar-Zadeh, Molybdenum oxides – from fundamentals to functionality, *Adv. Mater.*, 2017, **29**, 1701619.

33 W. Liu, C. Li, Q. Xu, P. Yan, C. Niu, Y. Shen, P. Yuan and Y. Jia, Anderson localization in 2D amorphous MoO_{3-x} monolayers for electrochemical ammonia synthesis, *ChemCatChem*, 2019, **11**, 5412–5416.

34 K. Ajito, L. A. Nagahara, D. A. Tryk, K. Hashimoto and A. Fujishima, Study of the photochromic properties of amorphous MoO_3 films using Raman microscopy, *J. Phys. Chem.*, 1995, **99**, 16383–16388.

35 S. Balendhran, J. Deng, J. Z. Ou, S. Walia, J. Scott, J. Tang, K. L. Wang, M. R. Field, S. Russo, S. Zhuiykov, M. S. Strano, N. Medhekar, S. Sriram, M. Bhaskaran and K. Kalantar-zadeh, Enhanced charge carrier mobility in two-dimensional high dielectric molybdenum oxide, *Adv. Mater.*, 2013, **25**, 109–114.

36 J. Li, Y. Ye, L. Ye, F. Su, Z. Ma, J. Huang, H. Xie, D. E. Doronkin, A. Zimina, J.-D. Grunwaldt and Y. Zhou, Sunlight induced photo-thermal synergistic catalytic CO_2 conversion via localized surface plasmon resonance of MoO_{3-x}, *J. Mater. Chem. A*, 2019, **7**, 2821–2830.

37 W. Liu, Q. Xu, P. Yan, J. Chen, Y. Du, S. Chu and J. Wang, Fabrication of a single-atom platinum catalyst for the hydrogen evolution reaction: a new protocol by utilization of H_xMoO_{3-x} with plasmon resonance, *ChemCatChem*, 2018, **10**, 946–950.

38 Y. Li, X. Chen, M. Zhang, Y. Zhu, W. Ren, Z. Mei, M. Gu and F. Pan, Oxygen vacancy-rich MoO_{3-x} nanobelts for photocatalytic N_2 reduction to NH_3 in pure water, *Catal. Sci. Technol.*, 2019, **9**, 803–810.

39 A. R. Head, C. Gattinoni, L. Trotochaud, Y. Yu, O. Karslıoğlu, S. Pletincx, B. Eichhorn and H. Bluhm, Water (non-) interaction with MoO_3, *J. Phys. Chem. C*, 2019, **123**, 16836–16842.

40 Z. Luo, R. Miao, T. D. Huan, I. M. Mosa, A. S. Poyraz, W. Zhong, J. E. Cloud, D. A. Kriz, S. Thanneeru, J. He, Y. Zhang, R. Ramprasad and S. L. Suib, Mesoporous MoO_{3-x} material as an efficient electrocatalyst for hydrogen evolution reactions, *Adv. Energy Mater.*, 2016, **6**, 1600528.

41 T. Ge, Z. Wei, X. Zheng, P. Yan and Q. Xu, Atomic rearrangement and amorphization induced by carbon dioxide in two-dimensional MoO_{3-x} nanomaterials, *J. Phys. Chem. Lett.*, 2021, **12**, 6543–6550.

42 H. Cheng, X. Qian, Y. Kuwahara, K. Mori and H. Yamashita, A plasmonic molybdenum oxide hybrid with reversible tunability for visible-light-enhanced catalytic reactions, *Adv. Mater.*, 2015, **27**, 4616–4621.

43 H. Cheng, M. Wen, X. Ma, Y. Kuwahara, K. Mori, Y. Dai, B. Huang and H. Yamashita, Hydrogen doped metal oxide semiconductors with exceptional and tunable localized surface plasmon resonances, *J. Am. Chem. Soc.*, 2016, **138**, 9316–9324.

44 W. Liu and Q. Xu, Fabrication of Ag/h-MoO_3 with surface plasmon resonances for enhanced photoelectrochemical performance, *Sol. RRL*, 2019, **3**, 1900242.